Monthly Notices
of the
ROYAL ASTRONOMICAL SOCIETY

MNRAS **437,** 2607–2620 (2014) doi:10.1093/mnras/stt2072
Advance Access publication 2013 December 3

Low X-ray luminosity galaxy clusters – II. Optical properties and morphological content at $0.18 < z < 0.70$★

José Luis Nilo Castellón,[1,2†] M. Victoria Alonso,[1,3] Diego García Lambas,[1,3] Ana Laura O'Mill,[4] Carlos Valotto,[1,3] Eleazar R. Carrasco,[5] Héctor Cuevas[2] and Amelia Ramírez[2]

[1]*Instituto de Astronomía Teórica y Experimental, (IATE-CONICET), Laprida 922, Córdoba, Argentina*
[2]*Departamento de Física, Facultad de Ciencias, Universidad de La Serena, Cisternas 1200, La Serena, Chile*
[3]*Observatorio Astronómico de Córdoba, Universidad Nacional de Córdoba, Laprida 854, Córdoba, Argentina*
[4]*Instituto de Astronomia, Geofísica e Ciências Atmosféricas da USP, Rua do Matão 1226, Cidade Universitária, São Paulo, SP 05508-090, Brazil*
[5]*Gemini Observatory/AURA, Southern Operations Center, Casilla 603, La Serena, Chile*

Accepted 2013 October 23. Received 2013 October 23; in original form 2012 November 5

ABSTRACT

This is the second of a series of papers on low X-ray luminosity galaxy clusters, in which we present the r', g' and i' photometry obtained with Gemini Multi-Object Spectrograph IMAGE at Gemini North and South telescopes for seven systems in the redshift range of 0.18 to 0.70. Optical magnitudes, colours and morphological parameters, namely, concentration index, ellipticity and visual morphological classification, are also given. At lower redshifts, the presence of a well-defined red cluster sequence extending by more than 4 mag showed that these intermediate-mass clusters had reached a relaxed stage. This was confirmed by the small fraction of blue galaxy members observed in the central regions of ∼0.75 Mpc. In contrast, galaxy clusters at higher redshifts had a less important red cluster sequence. We also found that the galaxy radial density profiles in these clusters were well fitted by a single power law. At $0.18 < z < 0.70$, we observed an increasing fraction of blue galaxies and a decreasing fraction of lenticulars, with the early-type fraction remaining almost constant. Overall, the results of these intermediate-mass clusters are in agreement with those for high-mass clusters.

Key words: galaxies: clusters: general – galaxies: fundamental parameters – galaxies: photometry.

1 INTRODUCTION

Clusters of galaxies are ideal systems to investigate the assembly of the structures in the Universe. In massive clusters, Dressler et al. (1997) found significant changes in their morphological content as a function of redshift, with these results being explained by the major episodes of star formation produced in the galaxies at higher redshifts followed by a subsequent passive evolution with little star formation activity (Ellis et al. 1997; Gladders et al. 1998; Stanford, Eisenhardt & Dickinson 1998). Poggianti et al. (2009) showed that at redshifts of $0.5 < z < 1.2$, the morphological evolution was not only restricted to massive clusters. In lower mass systems, the fraction of spiral and S0 galaxies evolved more strongly while ellipticals remained unchanged.

Colour–magnitude relations (CMRs) were first used to find galaxy clusters and to estimate their redshifts (Yee, Gladders & López-Cruz 1999). Since then, the slope and scatter of this relation have been studied for different cluster samples with diverse masses and redshifts. For instance, changes in the CMR slope with redshift were able to constrain the formation epoch of galaxy clusters (Gladders et al. 1998). Mei et al. (2009) studied the CMR scatter to obtain the average age of early-type galaxies in the clusters, but found no significant dependence on cluster mass or redshift (e.g. Kodama & Arimoto 1997; Kauffmann & Charlot 1998; Bernardi et al. 2005; Gallazzi et al. 2006; Tran et al. 2007).

The red cluster sequence (hereafter, RCS) is a tight sequence in the colour–magnitude plane defined by early-type galaxies (Visvanathan & Sandage 1977; Gladders et al. 1998; De Lucia et al. 2004; Gilbank et al. 2008; Lerchster et al. 2011), which was used by Mullis et al. (2005) as a reliable distance indicator of massive, X-ray-luminous galaxy clusters at $z \sim 1.4$. In addition, Demarco

★ Based on observations obtained at the Gemini Observatory, which is operated by Association of Universities for Research in Astronomy, Inc., under cooperative agreement with the National Science Foundation (NSF) on behalf of the Gemini partnership: the NSF (USA), the Particle Physics and Astronomy Research Council (Canada), CONICYT (Chile), the Australian Research Council (Australia), CNPq (Brazil) and CONICET (Argentina).

† E-mail: josenilocastellon@gmail.com

Table 1. Low X-ray luminosity galaxy clusters.

[VMF98] Id.	Right ascension (J2000)	Declination (J2000)	L_X (10^{43} cgs)	z	Program Id.	g'	r'	i'
001	00 30 33.2	+26 18 19	26.1	0.500	GN-2010B-Q-73	–	15 × 300	15 × 150
022	02 06 23.4	+15 11 16	3.6	0.248	GN-2003B-Q-10	–	4 × 300	4 × 150
093	10 53 18.4	+57 20 47	1.4	0.340	GN-2011A-Q-75	–	5 × 600	4 × 150
097	11 17 26.1	+07 43 35	6.4	0.477	GS-2003A-SV-206	12 × 600	7 × 900	–
119	12 21 24.5	+49 18 13	42.7	0.700	GN-2011A-Q-75	–	7 × 190	4 × 120
124	12 52 05.4	−29 20 46	3.4	0.188	GS-2003A-SV-206	5 × 300	5 × 600	–
148	13 42 49.1	+40 28 11	16.2	0.699	GN-2011A-Q-75	–	7 × 190	5 × 120

et al. (2010) confirmed some red sequence galaxy clusters spectroscopically at redshifts higher than 1.

Low X-ray luminosity (i.e. intermediate-mass) clusters have not been extensively studied compared to massive, luminous X-ray systems. Among these existing few studies, Balogh et al. (2002) found that in intermediate X-ray luminosity clusters at $0.23 < z < 0.3$, the galaxy properties are similar to those in massive clusters at the same redshift range. Moreover, Jeltema et al. (2006) found scaling relations between luminosity, temperature and velocity dispersion in six groups at $0.2 < z < 0.6$, which were comparable to those observed in nearby galaxy systems. Carrasco et al. (2007) studied the low luminosity X-ray cluster RX J1117.4+0743 at $z = 0.485$ and reported a complex morphology existing composed of at least two substructures in velocity space. This cluster also presented an offset between the position of the brightest group galaxy and the X-ray emission centre.

More recently, Balogh et al. (2011) conducted a morphological study of similar clusters at $0.85 < z < 1$, providing more evidence that group environment plays an important role in galaxy evolution. Based on colours, a prominent transient population was identified which moved from the blue cloud to the red sequence. In addition, Connelly et al. (2012) presented an extensive spectroscopic study of X-ray and optically defined systems at intermediate redshifts, which contributed to the understanding of galaxy evolution, in particular through the L_X–σ relation of these systems.

Our aim is to shed new light on the cluster assembly of low X-ray luminosity galaxy clusters within the hierarchical formation scenario. The first paper of the series (Nilo Castellón et al. 2013, hereafter Paper I) contained the main goals, sample selection, and details of observations and data reduction for both photometry and spectroscopy. Membership was defined as galaxies with projected distances of less than 0.75 Mpc from the cluster centre. For galaxy clusters observed with spectroscopy, membership was also restricted to objects having differences in radial velocities (ΔV) relative to the mean cluster smaller than the cluster velocity dispersion. For those clusters without any available spectroscopy, we used the studies of O'Mill et al. (2012) and Aihara et al. (2011) to estimate the photometric redshifts for all objects in the cluster fields. Following Paper I, taking into account higher uncertainties in the photometric redshift estimates, members had ΔV values of approximately 6000 km s^{-1}.

Here, in this second paper, we present the photometric properties of seven low X-ray luminosity, intermediate-mass galaxy clusters observed with Gemini telescopes. In Section 2, we present the photometric data and morphological parameters of the cluster members, together with an example of the catalogue. In Section 3, we analyse photometric properties namely galaxy number counts, CMRs with the RCS and colours, galaxy number density profiles, galaxy projected distributions and morphological content. In Section 4, we present a summary of the main results for these seven intermediate-mass galaxy clusters.

For all cosmology-dependent calculations, we assume $\Omega_\Lambda = 0.7$, $\Omega_m = 0.3$ and $h = 0.7$.

2 PHOTOMETRIC DATA

We selected 19 galaxy clusters from the *ROSAT* position sensitive proportional counters pointed observations (Vikhlinin et al. 1998; Mullis et al. 2003) for this project. These had X-ray luminosities in the range $L_X \sim 0.5$–45×10^{43} erg s^{-1}, angular core radius smaller than 60 arcsec and redshifts between 0.15 and 0.70 (for further details, see Paper I). The galaxy photometric properties of seven clusters observed with Gemini North and South telescopes using the Gemini Multi-Object Spectrograph (GMOS; Hook et al. 2004) in the image mode are presented. The detector is an array of three 2048 × 4608 pixels EEV CCDs, and using a 2 × 2 binning, the pixel scale is 0.1454 arcsec per pixel which corresponds to a field of view (FOV) of 5.5 arcmin^2 of the sky. This strategy allowed us to study about 1.2 Mpc of the cluster centre, regardless of the redshift.

All galaxy clusters and Landolt (1992) standard stars were observed using the r' filter; g' or i' filters were used to obtain colours. Table 1 shows a summary of the main characteristics of the clusters including the identification from Vikhlinin et al. (1998); the equatorial coordinates of the X-ray emission peak, the X-ray luminosity in the 0.5–2.0 keV energy band and also the mean redshift measured by Mullis et al. (2003) together with the Gemini Programme identification and the observing passbands (including number of exposures and individual exposure time in seconds, respectively). All images were observed under good photometric conditions with mean seeing values of 0.75, 0.66 and 0.74 arcsec in the g', r' and i' filters, respectively. The last observations (GN-2011A-Q-75) were taken under excellent conditions, with seeing in the r' band being between 0.48 and 0.55 arcsec.

The colour composed images obtained in the central parts of these studied clusters can be found in Paper I, where the standard reduction and galaxy detection are specified. These images were processed with the v1.4 Gemini IRAF[1] package, where they were overscanned and bias subtracted, as well as being trimmed and flat-fielded before being combined to create the final images. SExtractor v2.5.0 (Bertin & Arnouts 1996) was used for galaxy detection and to obtain the main photometric parameters. Using the star–galaxy separation, galaxies were defined as those objects having an isophotal axis ratio $b/a > 0.9$, CLASS_STAR < 0.8

[1] IRAF is distributed by NOAO, which is operated by the Association of Universities for Research in Astronomy Inc., under cooperative agreement with the NSF.

Table 2. Completeness levels in the r' band.

[VMF98] Identification	50 per cent level	90 per cent level
001	23.20 ± 0.04	23.70 ± 0.05
022	22.00 ± 0.09	23.00 ± 0.02
093	22.10 ± 0.07	23.00 ± 0.20
097	23.10 ± 0.02	24.00 ± 0.04
119	23.20 ± 0.06	23.70 ± 0.10
124	21.50 ± 0.04	23.00 ± 0.05
148	23.20 ± 0.08	23.60 ± 0.16

(a parameter associated with the light distribution) and half-light radius > 5 arcsec. The galaxy total magnitudes were of SExtractor Kron magnitude (MAG_AUTO) and the colours were aperture magnitudes obtained within a fixed aperture of 20 pixels (equivalent to 2.9 arcsec). The photometric procedure is extensively detailed in Paper I.

SExtractor overestimates the aperture magnitudes of the brightest galaxies in clusters, an effect which is particularly important at lower redshifts. For the bright objects in [VMF98]022 and [VMF98]124, we used aperture magnitudes within an 80 pixel radius as their total magnitudes. Final magnitudes were expressed in the AB system, after correcting for galactic extinction using reddening maps from Schlegel, Finkbeiner & Davis (1998). Magnitude limits and completeness levels for the galaxy clusters were obtained through simulated catalogues and images using the procedures explained in Paper I. Table 2 shows the r' magnitudes and their Poisson errors obtained for 50 and 90 per cent completeness levels in the studied fields. The deepest images corresponded to the best observation conditions mentioned above.

2.1 Morphological parameters

One of our main goals was to study galaxy morphology evolution in low- and intermediate-mass clusters. As mentioned by many authors (Fasano et al. 2000; van den Bergh 2001; Vulcani et al. 2010; Calvi, Poggianti & Vulcani 2011), a correct morphology assignment to a galaxy depends on several factors such as the observed instrumental properties, the passbands, the quality of the observations and galaxy redshifts, among others. The quality of our observations allowed us to resolve structures with sizes between 1.5 and 4 kpc according to the galaxy redshifts, and therefore it was possible to perform a morphological classification based on visual inspection. This classification was carried out by four members of our team (JLNC, MVA, HC, AR) using r' postage stamps with a fixed size of 50×50 kpc. No information concerning galaxy redshift, colours, cluster properties, or spectroscopic features was used.

Five different morphological types were defined. Elliptical galaxies ($T = 1$) were those objects having extended and bright haloes with a clear spheroidal morphology and without substructures or asymmetries. S0/Sa galaxies ($T = 2$) had extended haloes and bright but concentrated cores, and also included in this type were those galaxies with a clear edge-on lenticular shape. Spiral galaxies ($T = 3$) were objects with clear arms, or/and an extended and tight edge-on disc with bright cores. Irregulars ($T = 4$) were objects having no clear structures or possible mergers ($T = 5$).

Consistently, for about 71 per cent of galaxies, the same morphological type was assigned by the different observers. For 19 per cent of the cases, only two members of the team gave the same morphological type. To define the morphological type for those objects with no clear assignment, another classification was performed by using the observed images in all the filters and the combined image. This resulted in less than 2 per cent of the cases having no clear structure and being in general small-sized faint galaxies which were assigned $T = 4$. As an independent check on our procedure, we used the available spectra with good signal-to-noise ratio for 75 galaxies, taking into account the continuum spectral shape and some characteristic emission and/or absorption lines. The final assignment of galaxy type considered the spectral library of Kinney et al. (1996) finding a good agreement in 59 galaxies. Some examples of our morphological classification are given in Fig. 1. From top to bottom, shown are ellipticals, S0s, spirals and irregulars or peculiar galaxies. Synthetic images of 100 galaxies with different redshifts and morphologies were created consistently with the observational conditions using stuff and skymaker (explained in Paper I). These synthetic galaxies were then classified using the same criteria defined above, with there being no coincident morphology assignment only for 10 faint objects.

The concentration index (C) is a suitable measurement of galaxy structure, and due to it being a robust and easy way to measure objects automatically, it is ideal for large galaxy surveys (Conselice, Bershady & Jangren 2000; Strateva et al. 2001; Yamauchi et al. 2005). This parameter has been used as the first indicator of the galaxy morphology in various studies (Hashimoto & Oemler 1999; Yamauchi et al. 2005; Conselice, Rajgor & Myers 2008). However, using the *Hubble Space Telescope* Great Observatories Origins Deep Survey and Advanced Camera for Surveys and *Hubble Deep Field* images, Conselice (2003) has shown that the C parameter can only be reliably measured out to $z \sim 3$.

In this work, we used the concentration index as defined by the ratio of two circular radii which contain 80 and 20 per cent of the total Petrosian flux. In this way, centrally concentrated ellipticals presented larger C values compared with those of late-type galaxies. For a classical de Vaucouleurs profile, C is approximately 5, while for an exponential disc it has a value of about 2 (Conselice 2003). For our data, low values of C were found in general and presented a large scatter for each morphological type.

Fig. 2 shows the concentration index distributions for all galaxies visually classified as ellipticals, lenticulars and spirals. The left-hand panel contains the objects of the three lower redshift clusters, while the right-hand panel has objects from clusters at higher redshifts. In general, at lower redshifts, the distributions were in agreement with the normal properties of the three galaxy morphologies. The C distribution for early-type objects was well defined with a peak at about 2.8, whereas for higher redshifts this distribution was broader with several peaks between 2.4 and 3.5. After checking that galaxies with lower C values corresponded to objects with fainter r' total magnitudes, we were then able to use C, b/a and the visual morphological type T as suitable morphological parameters to study the photometric properties of the galaxies in these low X-ray clusters.

2.2 The final catalogues

As an example of the catalogues Table 3 shows the following photometric properties together with the redshift of the 26 member galaxies in the neighbourhoods of the cluster [VMF98]022: galaxy identification; J2000 equatorial coordinates; r' total magnitude and aperture colour (within 2.9 arcsec); structural parameters such as concentration index, ellipticity, visual classification and redshift. The catalogues from the studied clusters can be accessed at http://www.dfuls.cl/XGClusters/ (Nilo Castellon & Alonso 2013).

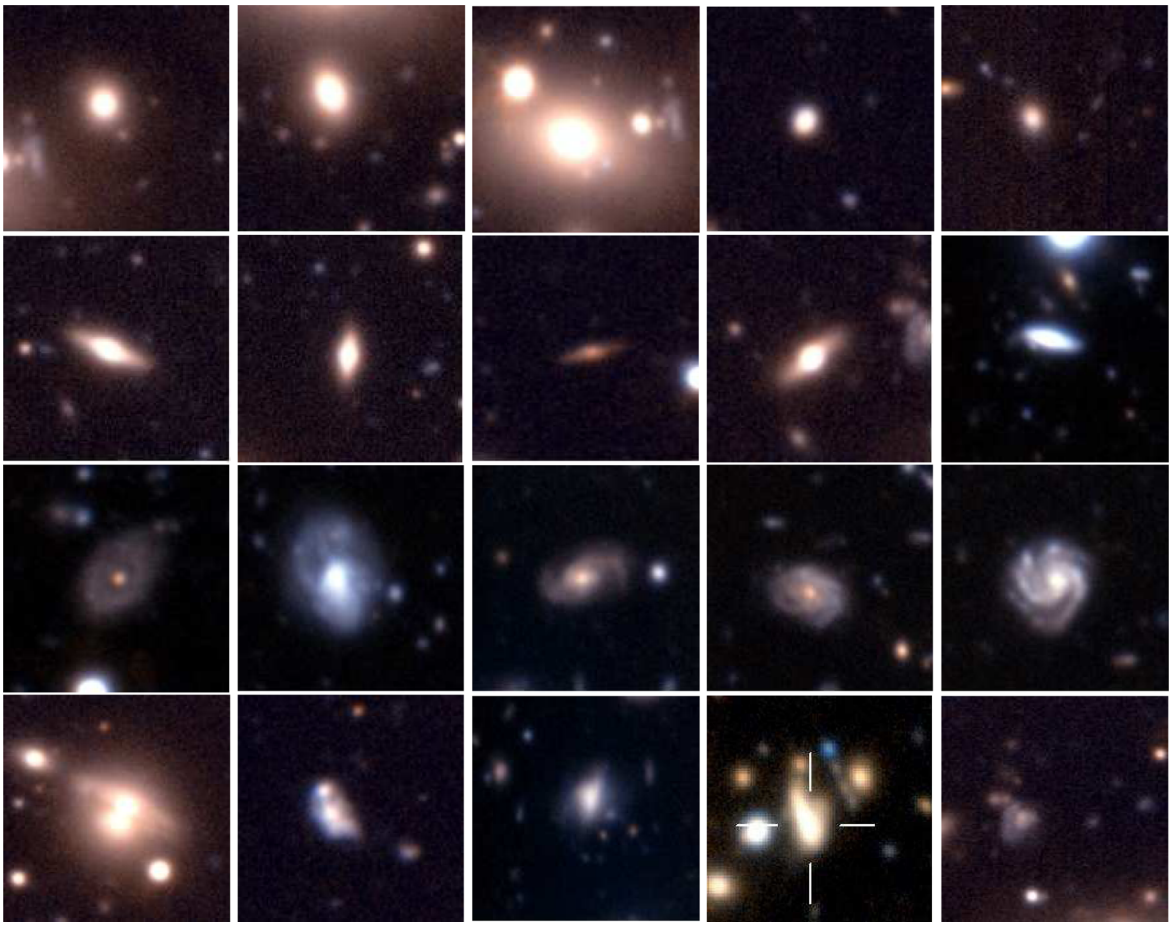

Figure 1. Morphological type classification. Some examples of galaxies classified in this paper, from top to bottom: ellipticals, lenticulars, spirals, irregulars and mergers/peculiars.

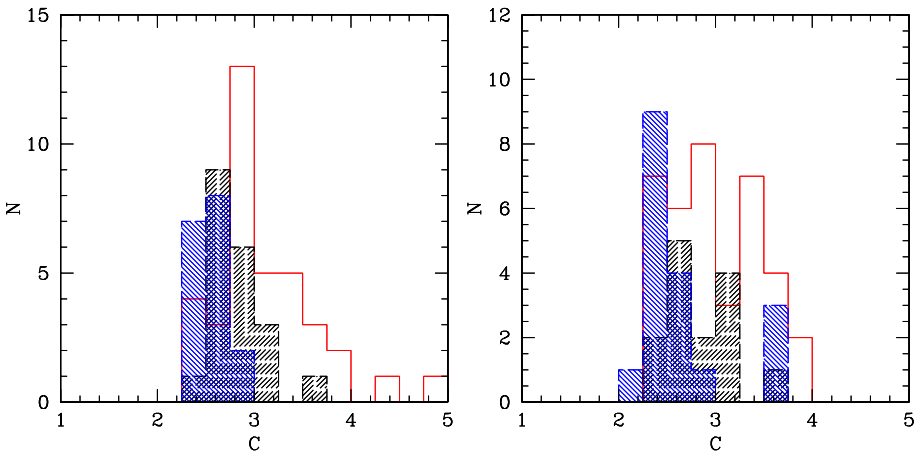

Figure 2. Concentration index distributions for all visually classified galaxies. Low- (high-) redshift clusters are shown in left- (right-) hand panels. Histogram colours correspond to ellipticals (red), lenticulars (black shaded) and spirals (blue).

As mentioned before, the magnitudes were given in the AB system, after being fully corrected by galactic extinction.

3 DATA ANALYSIS

We restricted our analysis to galaxies within 0.75 Mpc from the cluster centre, a limit that is small enough to include the virialized region of the studied clusters. Although a larger radii should be used for richer systems, for reasons of simplicity we adopted this radial cut at 0.75 Mpc, which removed the presence of a significant bias across the cluster sample due to the different weightings of external and internal regions. In this way, we were able to perform the same analysis on all the clusters regardless of their redshifts.

To determine cluster centres, two different criteria were used: the centre of a dominant galaxy (the bright custer galaxy, hereafter BCG, at least 1.5 mag brighter than the second ranked

Table 3. Galaxy member properties of the low X-ray luminosity cluster [VMF98]022.

Galaxy Id.	RA (J2000)	Dec. (J2000)	r'	$(r-i)'$	C	b/a	T	z
J020622.6+151132	02:06:22.698	+15:11:32.86	21.1415	0.6319	2.422	0.032	3	0.24680
J020631.8+151126	02:06:31.848	+15:11:26.73	22.2924	0.6706	2.543	0.321	2	0.24843
J020614.9+151125	02:06:14.981	+15:11:25.59	21.5822	0.5430	2.501	0.338	3	0.25017
J020621.9+151125	02:06:21.984	+15:11:25.54	19.4243	0.7473	3.246	0.038	1	0.25100
J020622.2+151120	02:06:22.277	+15:11:20.00	21.1816	0.6866	2.802	0.025	1	0.24878
J020615.3+151111	02:06:15.316	+15:11:11.29	20.7716	0.7061	2.686	0.273	2	0.24732
J020619.1+151107	02:06:19.175	+15:11:07.49	20.7354	0.7264	2.612	0.337	3	0.25040
J020621.2+151101	02:06:21.231	+15:11:01.58	17.9699	0.7517	4.448	0.196	1	0.24737
J020633.6+151101	02:06:33.613	+15:11:01.54	18.5363	0.7041	3.607	0.168	2	0.25032
J020617.4+151040	02:06:17.455	+15:10:40.28	19.9922	0.7202	3.386	0.072	1	0.24611
J020613.6+151035	02:06:13.667	+15:10:35.04	20.3462	0.7189	2.777	0.234	1	0.24630
J020617.6+151034	02:06:17.657	+15:10:34.60	21.7576	0.6954	2.552	0.203	3	0.24893
J020614.0+151031	02:06:14.061	+15:10:31.70	20.9661	0.7069	2.781	0.256	2	0.24870
J020613.1+150927	02:06:13.161	+15:09:27.30	20.2152	0.7201	2.661	0.242	2	0.25100
J020623.7+151327	02:06:23.735	+15:13:27.61	18.7835	0.7052	3.507	0.301	1	0.24715
J020628.8+151303	02:06:28.836	+15:13:03.25	21.8539	0.5855	2.428	0.032	2	0.25100
J020629.1+151254	02:06:29.119	+15:12:54.07	19.6068	0.6969	2.821	0.376	2	0.24857
J020628.0+151225	02:06:28.023	+15:12:25.28	21.4024	0.8439	2.801	0.679	3	0.24872
J020624.8+151214	02:06:24.830	+15:12:14.23	19.9894	0.6956	2.930	0.41	1	0.24389
J020624.4+151211	02:06:24.488	+15:12:11.01	20.9378	0.7046	2.651	0.287	2	0.24554
J020614.3+151210	02:06:14.362	+15:12:10.22	20.7151	0.6902	2.535	0.382	3	0.24854
J020630.4+151200	02:06:30.424	+15:12:00.25	19.1867	0.7230	3.315	0.195	1	0.25001
J020620.8+151158	02:06:20.852	+15:11:58.04	19.9817	0.7054	3.113	0.39	1	0.24899
J020634.0+151153	02:06:34.072	+15:11:53.80	20.0432	0.6971	2.739	0.302	1	0.24901
J020628.2+151153	02:06:28.258	+15:11:53.03	20.5783	0.7432	2.735	0.347	1	0.24830
J020625.4+151145	02:06:25.488	+15:11:45.94	21.3265	0.6721	2.875	0.092	5	0.24600

cluster galaxy) in the three low-redshift clusters ([VMF98]001, [VMF98]093 and [VMF98]124) and the peak of the X-ray emission in the four high-redshift clusters. In the first case, the difference between the peak of the X-ray emission and the BCG centre was less than the X-ray peak position uncertainty.

In this section, we used the photometric properties of the galaxies defined as members in the seven studied galaxy clusters. For galaxies with spectroscopic redshifts, cluster membership was assigned to galaxies with clustercentric radial velocity differences smaller than the velocity dispersion of the cluster. However, for those galaxies with only photometric redshift estimates, we considered as members those objects with radial velocity relative differences less than 6000 km s^{-1}.

3.1 Number counts

The r' number counts were defined as the number of galaxies in the magnitude range of 16 to 27 mag in 0.5 mag bins per square degrees. Our results were compared with models from Nagashima et al. (2002) for three different cosmologies: a standard cold dark matter universe (SC), a low-density flat universe with a non-zero cosmological constant (LC) and a low-density open universe with zero cosmological constant (OC). The photometric relations were taken from Fukugita, Shimasaku & Ichikawa (1995) and incorporated into the models after being transformed to our photometric system.

Fig. 3 shows r' number counts on the logarithmic scale for all the galaxies in the GMOS FOV for the seven galaxy clusters, with error bars being estimated using Poisson uncertainties. Models from Nagashima et al. (2002) are also shown, with those with selection effects being represented by thick lines, while models without selection effects are shown by thin lines. A large scatter can be observed in the number counts at brighter magnitudes and a strong

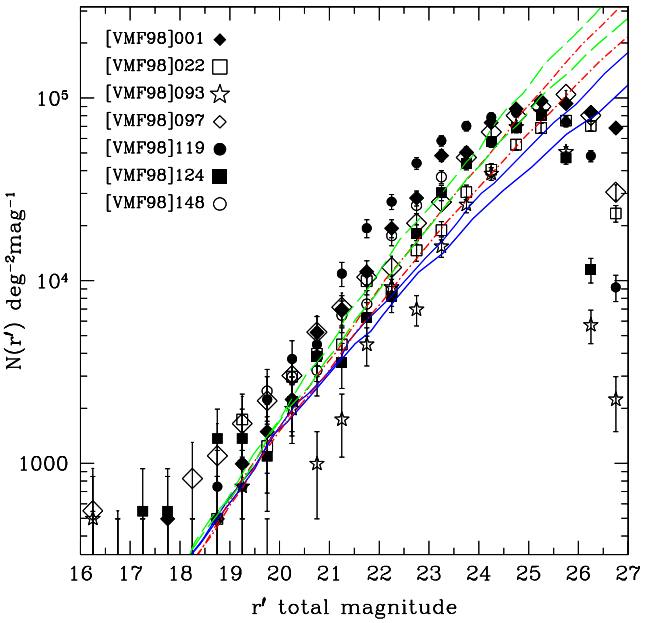

Figure 3. Number counts in the r' band for the galaxy clusters. Models from Nagashima et al. (2002) are included. Thick (thin) lines represent those models with (without) selection effects. The three models: SC, OC and LC are exhibited with different line types (see the text for details).

decay beyond 25 mag. Also, an excess at fainter magnitudes may be seen associated with the blue faint excess found by Bruzual & Kron (1980) and King & Ellis (1985).

In general, the observed number counts were slightly higher than those from the models, as expected due to the presence of clusters in the fields. The number counts at a fixed $r' = 22$ mag range between

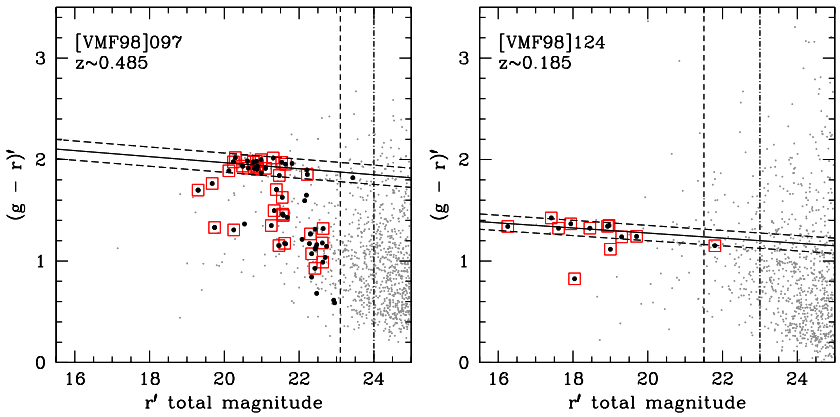

Figure 4. $(g-r)'$ CMRs in the neighbourhoods of the galaxy clusters. Small grey dots represent objects classified as galaxies. Big black dots correspond to galaxies with photometric redshifts. Open symbols are those confirmed cluster members with spectroscopic data (squares) or photometric redshifts (triangles). Vertical dashed lines correspond to limiting magnitudes with 90 and 50 per cent completeness levels. The linear RCS regressions (solid line) within uncertainties are also shown.

5×10^3 and 2×10^4 (clusters [VMF98]093 and [VMF98]119, respectively), consistent with their X-ray luminosities (see Table 1).

Linear regressions were also obtained of the number counts between $19 < r' < 24$ with a slope in the range 0.3 to 0.43, consistent with the typical value of about 0.37 found by Metcalfe et al. (2001) in the regime of $20 < R < 26$ mag. We noticed that the different passbands and adopted techniques, along with the assumptions and completeness corrections made it difficult to compare these results with other authors.

3.2 The colour–magnitude relation

Fig. 4 shows the $(g-r)'$ CMRs for the clusters [VMF98]097 and [VMF98]124, and in Fig. 5 are the $(r-i)'$ CMRs for [VMF98]001, [VMF98]022, [VMF98]093, [VMF98]119 and [VMF98]148. Small black dots represent objects classified as galaxies according to our photometric criteria (Paper I), implying that they had a semiminor to semimajor axis ratio higher than 0.9, an SExtractor CLASS_STAR smaller than 0.8 and a half-light radius bigger than 5 arcsec. Big black dots correspond to galaxies with photometric redshifts, with open squares representing members of the three galaxy clusters after applying the spectroscopic redshift criteria. This resulted in 26 confirmed galaxy members for [VMF98]022, 37 for [VMF98]097 and 12 for [VMF98]124 (Paper I). Open triangles represent cluster members defined using photometric redshift criteria, with 22, 14, 20 and 16 members being found for the clusters [VMF98]001, [VMF98]093, [VMF98]119 and [VMF98]148, respectively. Vertical dashed lines correspond to our limiting magnitudes with 90 and 50 per cent completeness levels, as defined in Paper I. The linear RCS regressions within uncertainties, as described below, are also shown in the figures.

The colours $(g-r)'$ in the redshift range of $0.1 < z < 0.5$ and $(r-i)'$ for $z > 0.5$ covered the 4000 Å break due to the passband width. Moreover, this allowed us to separate red early-type galaxies from star-forming objects at lower redshifts (0.25 to 0.35). In this way, we were able to distinguish the red sequence and star-forming galaxies (Bruzual 1983; Dressler & Shectman 1987). *K*-corrections were not applied to our magnitudes as we had photometric information in only two passbands and therefore corrections would have been approximate. Also, using tabular values, as for instance those from Frei & Gunn (1994) would only give rough estimates due to uncertainties in our morphological estimates.

3.2.1 *Red cluster sequence*

On inspection of the CMRs of Figs 4 and 5, a variety of RCSs can be observed. For low-redshift clusters, the presence of a well-defined RCS with an extension of 4 to 6 mag may be seen. This trend is the main characteristic of virialized systems with a dominant elliptical galaxy, which has low signatures of star formation. However, in cluster [VMF98]124 a range of about 2 mag without cluster members can be observed, with comparable RCS results also being found by Gladders et al. (1998) in their sample of lower redshift clusters and by Stott et al. (2009) and Gladders & Yee (2005). Steeper slopes were reported by Wake et al. (2005) for the RCS in poor galaxy clusters at lower redshifts, with the dispersion attributed to uncertainties in the definition of galaxy members.

Mei et al. (2006a,b) studied massive galaxy clusters at higher redshifts ($z > 1$) and focused on the RCS. Their reported slopes ranging -0.02 to -0.03 with the early-type red sequence being well defined out to redshifts of about 1.3 (Mei et al. 2009). For the higher redshift clusters, we found an RCS with an extension of about 2 to 4 mag, with these clusters presenting a different behaviour than the lower redshift clusters, revealing a mix of early-type galaxies together with more blue galaxies. This result is in agreement with that reported by De Lucia et al. (2007) in a study on massive clusters at $z > 0.8$ and that of a galaxy cluster at $z > 1$ reported by Lerchster et al. (2011). At these redshifts, however, it is difficult to compare results from different studies, because most of these were based on massive galaxy clusters.

As Gladders et al. (1998) noted, a lot of care has to be taken in the selection of the RCS galaxies, with, the total extension of the RCS and its scatter having been discussed by several authors for different types of clusters. For instance, Terlevich, Caldwell & Bower (2001) and Secker, Harris & Plummer (1997) defined an 8 mag RCS for the nearby clusters of Virgo and Coma. At redshifts of ∼0.15, Carrasco, Mendes de Oliveira & Infante (2006) determined the galaxy cluster RCS to be of 6 mag and even reaching 10 mag with a set of four groups and fossils. For low-mass clusters, Balogh et al. (2009) reported a 6 mag RCS using a spectroscopic sample of 10 groups between $z \sim 0.2$ and 0.3. In addition, at higher redshifts, De Lucia et al. (2006) identified an RCS extension of 6 mag for clusters at $z \sim 0.5$, and of 4 mag for those at $z \sim 0.8$, using the ESO Distant Clusters Survey sample. Based on these previous results, we chose to define the RCS as those cluster members which were 3 mag fainter

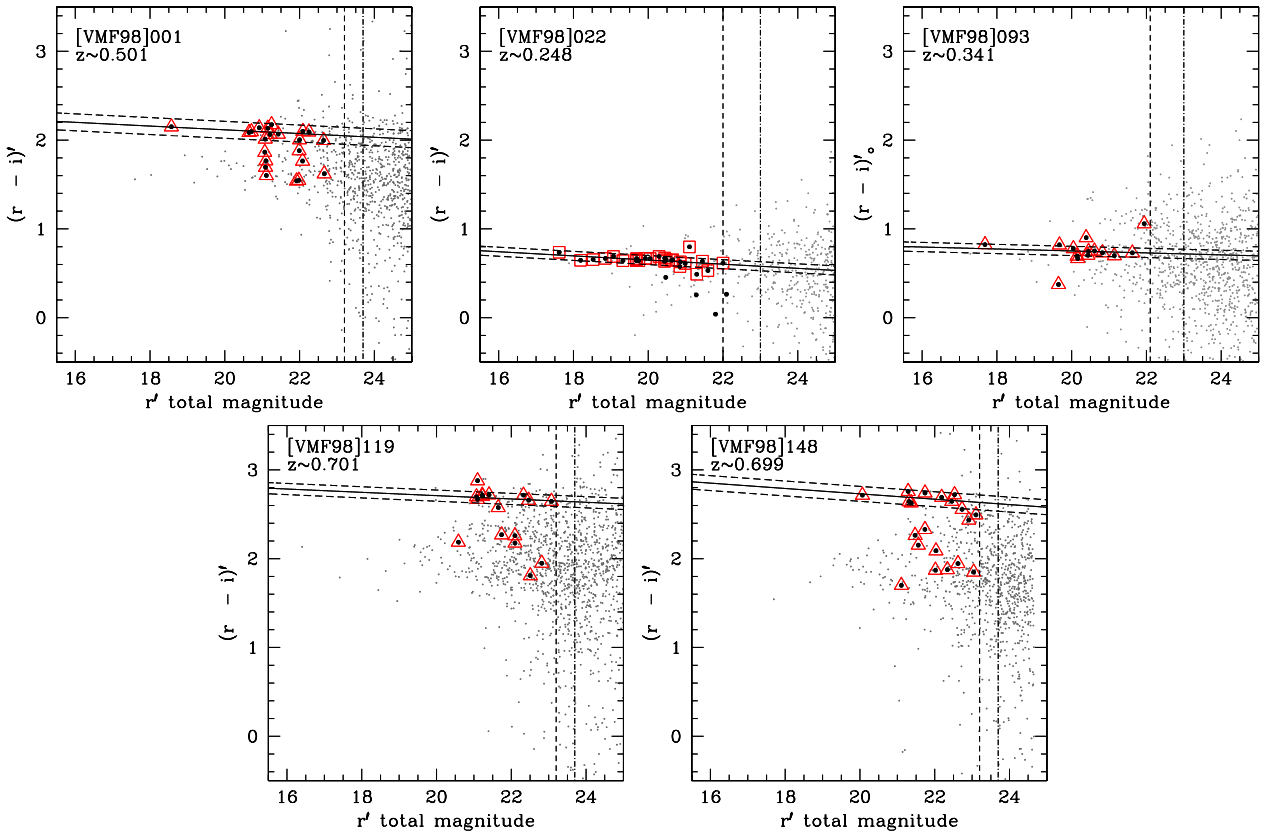

Figure 5. $(r-i)'$ CMRs in the neighbourhoods of the galaxy clusters. Symbols are explained in previous figures.

than the second brightest galaxy in the cluster, avoiding the BCG. This limit corresponded to approximately a 90 per cent magnitude completeness level, which is represented by vertical short dashed lines in the panels of the figures. For those clusters with a less clear RCS (see Figs 4 and 5), we selected early-type objects using only the redder galaxies at the cluster core which had a projected radius of about 0.3 Mpc (following Sarazin 1986), concentration index higher than 2.5 and ellipticities lower than 0.4 or $0.7 < b/a < 0.9$. In this way, we studied the central parts of the clusters dominated by red spheroidal galaxies, thus reducing foreground/background contamination.

Several authors have studied the performance of different techniques to fit the RCS, to provide estimates of the slope and zero-point (Press et al. 1992; van Dokkum et al. 1998; López-Cruz, Barkhouse & Yee 2004; Stott et al. 2009; Hao et al. 2010). Gladders et al. (1998) argue that linear regression plus an iterated 3σ clipping provides the most stable results. We followed this technique, but applied a 1σ clipping iteration to create a more conservative RCS sample. Then, using a least-squares regression, the RCS slope and zero-point were obtained, with errors being estimated using 10.000 bootstrap resampling. Table 4 shows the RCS number of galaxies and the slope and zero-point with their corresponding uncertainties for each cluster. The derived RCS slopes had a mean of approximately 0.02 with a spread of about 0.01.

Taking into account the linear fit regressions, for each cluster we defined the galaxy samples with colours over and below (within 1σ) the RCS sample. Hereafter, the Blue sample is defined as those galaxies with colours below the RCS, and will be used for further analysis in the following sections.

Table 4. Red cluster sequence: linear regressions.

[VMF98] Id.	Number of galaxies	Slope	Zero-point
001	13	-0.021 ± 0.006	2.537 ± 0.011
022	21	-0.023 ± 0.099	0.065 ± 0.011
093	10	-0.011 ± 0.017	0.084 ± 0.010
097	19	-0.029 ± 0.008	1.932 ± 0.012
119	8	-0.019 ± 0.006	3.083 ± 0.016
124	10	-0.025 ± 0.013	1.328 ± 0.019
148	10	-0.030 ± 0.011	3.335 ± 0.019

3.2.2 *Colours*

The colour distribution of the galaxy members was analysed for the seven clusters studied. For each distribution, we performed a statistical analysis considering both a single distribution for the whole galaxy sample and two Gaussian distributions for the RCS and blue samples. Figs 6 and 7 show the colour distributions for the cluster members with the dashed black curve corresponding to the single Gaussian distribution, while the blue and red curves indicate the two distributions. It was found that the single distribution was not a good representation of the colour distribution, and it was not possible to fit the blue population with reasonable precision for the three low-redshift clusters [VMF98]022; [VMF98]093 and [VMF98]124 due to the small number of blue galaxies. The observed $(r-i)'$ colours in the first two clusters may have been responsible for this small number in this low-redshift range. However, for [VMF98]124, the lowest redshift studied cluster, the GMOS FOV allowed us to study

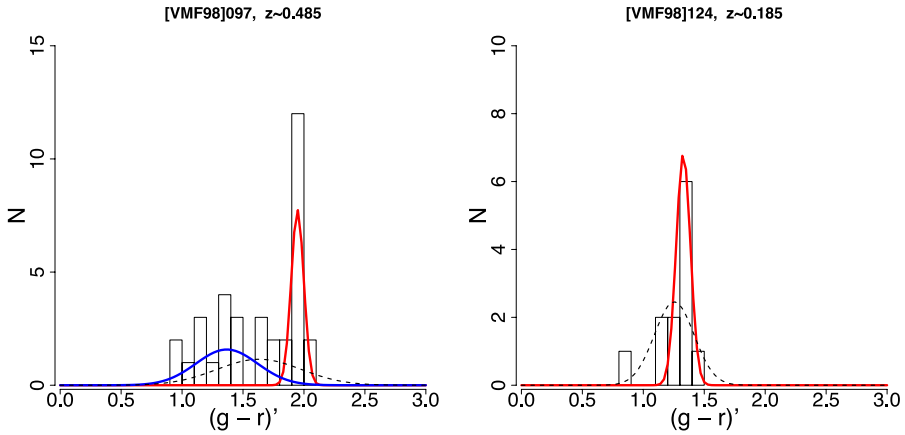

Figure 6. $(g-r)'$ colour distribution for the cluster galaxy members. Single fits are displayed: dashed black distribution represents the total member galaxies, in colours are shown the red and blue galaxy samples.

in detail the central parts by avoiding the blue galaxies in the outer parts.

Some galaxies had extreme colour values of around $(g-r)' \sim 0.8$ in [VMF98]124 and $(r-i)' \sim 0.37$ in [VMF98]093, which corresponded to approximately 5σ of the RCS fit (Fig. 4). In general, the blue excess was a good indicator of strong star formation in galaxies, with this effect possibly being related to cluster dynamics. McIntosh, Rix & Caldwell (2004) studied extreme colour galaxies and reported that they are spatially, kinematically and morphologically distinct from red cluster galaxies. Despite the colour of these galaxies, they were spectroscopically confirmed as cluster members, and are therefore genuine members of the original samples.

Table 5 shows the statistical results for the red and blue populations: mean values, standard deviation and χ^2 of the colour distribution of galaxy members. Despite the differences in the observed filters, there was an absence of blue galaxies at lower redshifts, with a red population occurring with a peak at $(g-r)' \sim 1.33$ for cluster [VMF98]124 and $(r-i)' \sim 0.64$ and 0.76 for clusters [VMF]022 and [VMF98]093, respectively. At higher redshifts, there were two clear colour populations in the four galaxy clusters, probably due to a mix of red and blue galaxy populations, thus suggesting a dynamically active cluster in the case of [VMF98]097 (Carrasco et al. 2007).

3.2.3 The Butcher–Oemler effect

This effect (Butcher & Oemler 1978) is related to the fraction of blue galaxies (f_b) in clusters, and its evolution over the last 6 Gyr. We calculated f_b in our galaxy clusters as the number of blue galaxies in the total distribution and compared our results with Kodama & Bower (2001), Fairley et al. (2002), de Lucia et al. (2007) and Barrena et al. (2012) in the same redshift range ($0.1 < z < 0.5$), cluster region ($r_p < 0.75$ Mpc) and equivalent colours. Fig. 8 shows the blue fraction as a function of redshift for our cluster sample (filled circles) along with those from the literature. For both our data and those of the literature, a consistent increase can be observed in the blue fraction of galaxies from lower redshift clusters compared to those at higher redshifts. These values were related with a 97 per cent confidence using the Kendall τ rank correlation coefficient. This larger fraction of blue galaxies in higher redshift clusters can also be seen in Figs 4 and 5. The larger uncertainties in higher redshift clusters could be due to sample selection or a larger mass spread of the clusters, among other factors.

3.3 Galaxy number density profiles

The galaxy number density profile was determined within a total area of radius ∼1.2 Mpc for our cluster sample. For the three lower redshift clusters the centre was defined by the BCG, whereas for the higher redshift clusters it was defined as the peak of the X-ray emission. The number density profiles were obtained for the two galaxy samples defined in the previous section: the RCS and the Blue samples. We also calculated the total radial galaxy number density profile for all member galaxies and we fitted power laws ($\rho(r) = Ar^{-\alpha}$) to the radial density profiles, obtaining α values from −0.65 for [VMF98]022 to −1.37 for [VMF98]001. Table 6 shows these values and the rms for the seven galaxy clusters, which are in the range reported by other authors (typical values from −0.7 to −1.4; Hansen et al. 2005). Figs 9 and 10 show the galaxy number density (ρ_c) profile as a function of the distance to the cluster centre (r_c) for low- and high-redshift clusters, respectively. The RCS (in red) and Blue samples are shown within statistical Poisson errors and are represented by the shaded areas. In addition, the total radial number density profile in logarithmic scale together with the power-law fit are included in the inner small panel. A central concentration for the RCS sample with an absence of blue galaxies can be observed for the three low-redshift clusters. About 70 per cent of the red galaxies were located in the cluster core ($r_c <$ 0.2 Mpc). However, a different behaviour was noted for the high-redshift galaxy clusters, where a remarkable increase in the number of blue galaxies was present, mainly at the centre. This could also be seen as an excess of blue galaxies in the colour–magnitude diagrams (Figs 4 and 5) related to the Butcher–Oemler effect (Fig. 8).

3.4 Galaxy projected distribution

The galaxy projected distribution was generated using the lattice package of the R software environment,[2] with Figs 11 and 12 showing the galaxy projected distribution for the three low-redshift and four high-redshift galaxy clusters, respectively. The contour maps are based on the RCS and Blue samples using open triangles and squares with the same symbol convention used in previous figures. In addition, crosses indicate the position of the X-ray emission

[2] R is a language and environment for statistical computing and graphics, designed by Robert Gentleman and Ross Ihaka of the Statistics Department of the University of Auckland; http://www.r-project.org/.

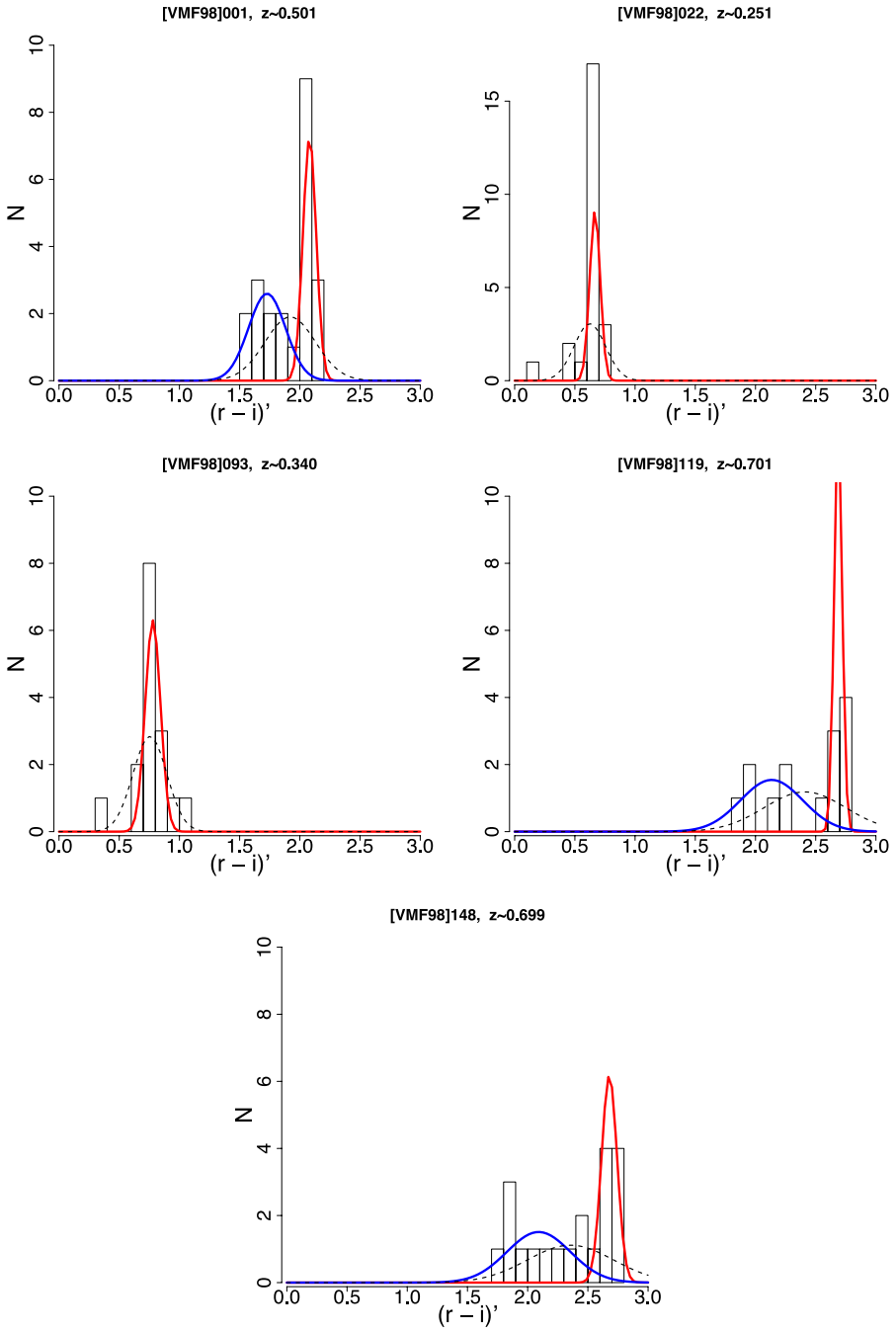

Figure 7. $(r-i)'$ colour distribution for the cluster galaxy members. Single fits are displayed as in previous figures.

Table 5. Gaussian fits to the galaxy populations: Statistical values.

[VMF98] Id.	Red mean	Population standard deviation	χ^2	Blue mean	Population standard deviation	χ^2
001	2.080	0.051	0.040	1.752	0.167	0.545
022	0.647	0.025	0.599	–	–	–
093	0.760	0.043	0.396	–	–	–
097	1.941	0.037	0.736	1.463	0.311	1.083
119	2.686	0.033	0.598	2.134	0.258	0.280
124	1.328	0.058	0.292	–	–	–
148	2.678	0.064	0.280	2.091	0.264	0.600

peak, filled triangles and squares show the BCG locus, with black dots corresponding to foreground and background galaxies. In the figures, north is up and east is to the left.

The figures reveal differences in the nature of the galaxy distribution. At lower redshifts, the cluster [VMF98]022 was centrally concentrated, but shows an elongated distribution in the northeast–southwest (NE–SW) direction. The central galaxy was located at (RA = $02^{h}06^{m}21^{s}$, Dec. = $15^{\circ}11'00''$), presenting a shift of ∼12 arcsec in the SW direction with respect to the X-ray peak emission where four red galaxies were located. The clusters [VMF98]093 and [VMF98]124 presented a smooth single distribution, with these results also being consistent with the well-defined RCS found for clusters [VMF98]022 and [VMF98]124 (Figs 4

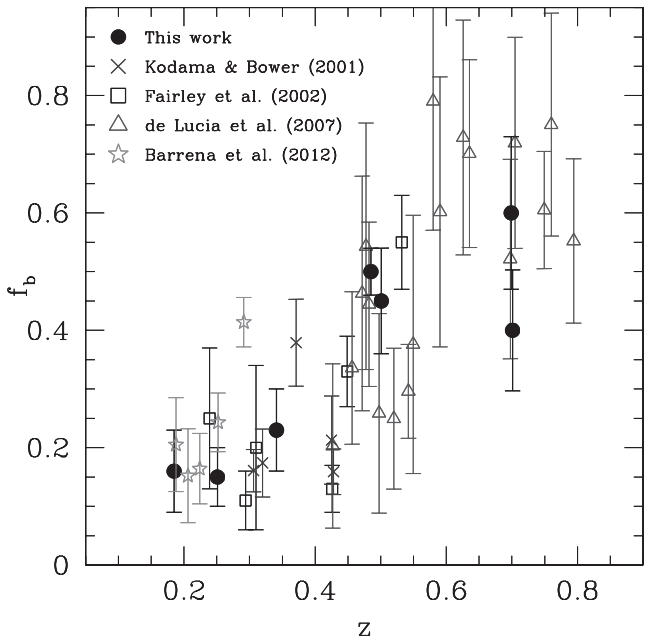

Figure 8. Butcher–Oemler effect for the studied galaxy clusters (filled circles). Blue fraction from galaxy clusters with X-ray luminosity of about 10^{44} ergs s^{-1} from Kodama & Bower (2001, crosses), Fairley et al. (2002, squares), de Lucia et al. (2007, triangles) and Barrena et al. (2012, stars) are also included.

Table 6. The α parameter of the power-law fit.

[VMF98] Id.	α	rms
001	-1.371 ± 0.285	2.323 ± 0.473
022	-0.519 ± 0.101	1.785 ± 0.350
093	-0.608 ± 0.162	2.001 ± 0.535
097	-0.908 ± 0.163	1.700 ± 0.305
124	-0.945 ± 0.272	2.020 ± 0.583
119	-1.212 ± 0.323	2.299 ± 0.614
148	-1.182 ± 0.264	2.281 ± 0.510

and 5, respectively). In these three lower redshift clusters, the cores were dominated by red galaxies in agreement with the typical morphology–density relation (Dressler et al. 1997) found for massive clusters. At higher redshifts, Fig. 12 reveals that the cluster [VMF98]097 had a better resolution, due to spectroscopic redshifts, compared to the other three galaxy clusters with photometric redshift estimates.

Both the present-day dynamic properties of clusters and the morphology of their member galaxies are believed to be strongly linked to the cluster accretion history (Tonnesen & Bryan 2009; Girardi et al. 2011). Relics of this process can be found in the form of substructures in the galaxy distribution, since they maintain a memory of past merger events (White, Cohn & Smit 2010).

The Dressler–Shectman test (DST; Dressler & Shectman 1988) evaluates the substructure in the velocity kinematics of galaxy groups identified in clusters in projection. By considering the number of neighbours in projection from each galaxy, the mean local velocity and the local velocity dispersion can be inferred, which can then be compared with the values for the whole group. This test has been used both in studies on individual clusters, e.g. Boschin et al. (2006), Girardi et al. (2008), Barrena et al. (2011) and in samples of clusters at different redshifts (Connelly et al. 2012; Einasto et al. 2012), as well as being utilized in numerical simulations (Knebe & Müller 2000; Cohn 2012).

Connelly et al. (2012) discussed the importance of defining the correct radial cut in order to define substructures in galaxy clusters. They found little dynamical complexity when using X-ray based r_{200} cuts whereas at larger radii (1 Mpc or greater) significantly more dynamical substructure was obtained using the DST. On applying this test to the three clusters with spectroscopic redshifts, we found a lack of significant substructure, an expected result due to the restriction of our study to the central, mostly virialized 0.75 Mpc region where less substructure is expected.

The [VMF98]097 cluster presented at least three overdensities, as shown on the contour map of Fig. 10. In Paper I, we reported the radial velocity distribution for this cluster and ruled out a Gaussian distribution (Hou et al. 2009). As seen in this figure, the cluster core of the high-redshift clusters did not have a dominant galaxy population, suggesting a mix of galaxies, as also observed in Figs 4 and 5. Carrasco et al. (2007) also studied this cluster [VMF98]097 and observed signs of dynamical complexity, while the density map presented here is slightly different as we analysed the inner 0.75 Mpc central region.

3.5 Morphological content

In Section 2.1, we discussed the visual morphological classification procedure and the adopted morphological parameters. It was found that 97 per cent of the galaxies classified as early types presented C values higher than 2.5, whereas for spiral galaxies, 98 per cent had values lower than 3.0, with S0/Sa galaxies presenting values between $2.5 < C < 3.6$. These distributions are illustrated in Fig. 2.

Fig. 13 shows the average C values for the early, lenticular and spiral types for each galaxy cluster as a function of the cluster redshift (left-hand panel). An increase in C was observed for early-type and lenticular galaxies, which may have been related to the presence of giant galaxies in the low-redshift clusters ($C > 4$). In contrast, for late types, we found smaller C values for the lower redshift cluster. The right-hand panel of the figure shows the fraction of these three morphological types relative to the total, with there being a clear trend corresponding to an increase in the number of lenticulars at lower redshifts. This effect in low-mass galaxy clusters was predicted by Poggianti et al. (2009) and Dressler et al. (2009) and our data seem to confirm this.

4 SUMMARY OF THE MAIN RESULTS

In this paper, we have presented the r', g' and i' photometry obtained with GMOS-IMAGE at Gemini North and South telescopes for seven low X-ray galaxy clusters: [VMF98]001, [VMF98]022, [VMF98]093, [VMF98]097, [VMF98]119, [VMF98]124 and [VMF98]148 in the redshift range of 0.18 to 0.70. We have reduced the images and created catalogues with the detected objects being classified as extended following our criteria discussed in Section 2. These catalogues contain the object coordinates, optical properties and redshift. In addition, magnitudes, colours and morphological parameters such as the concentration index, ellipticity and morphological type estimates are also included in the photometric properties. This work is the second in a series of papers aimed at understanding the processes involved in the formation and evolution of low X-ray luminosity galaxy clusters at intermediate redshifts.

The RCS and the Blue samples were defined using the cluster members as described in Section 3.2 and in Paper I. In our analysis,

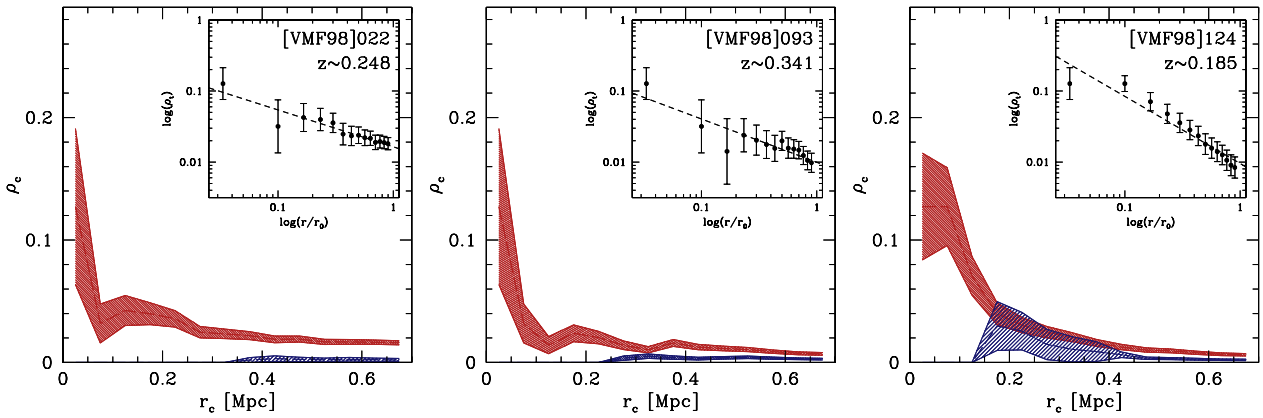

Figure 9. Galaxy number density profiles for the low-redshift galaxy clusters for the RCS (red) and Blue (blue) samples. The total radial galaxy number density profiles are shown in the small panel (see the text for details).

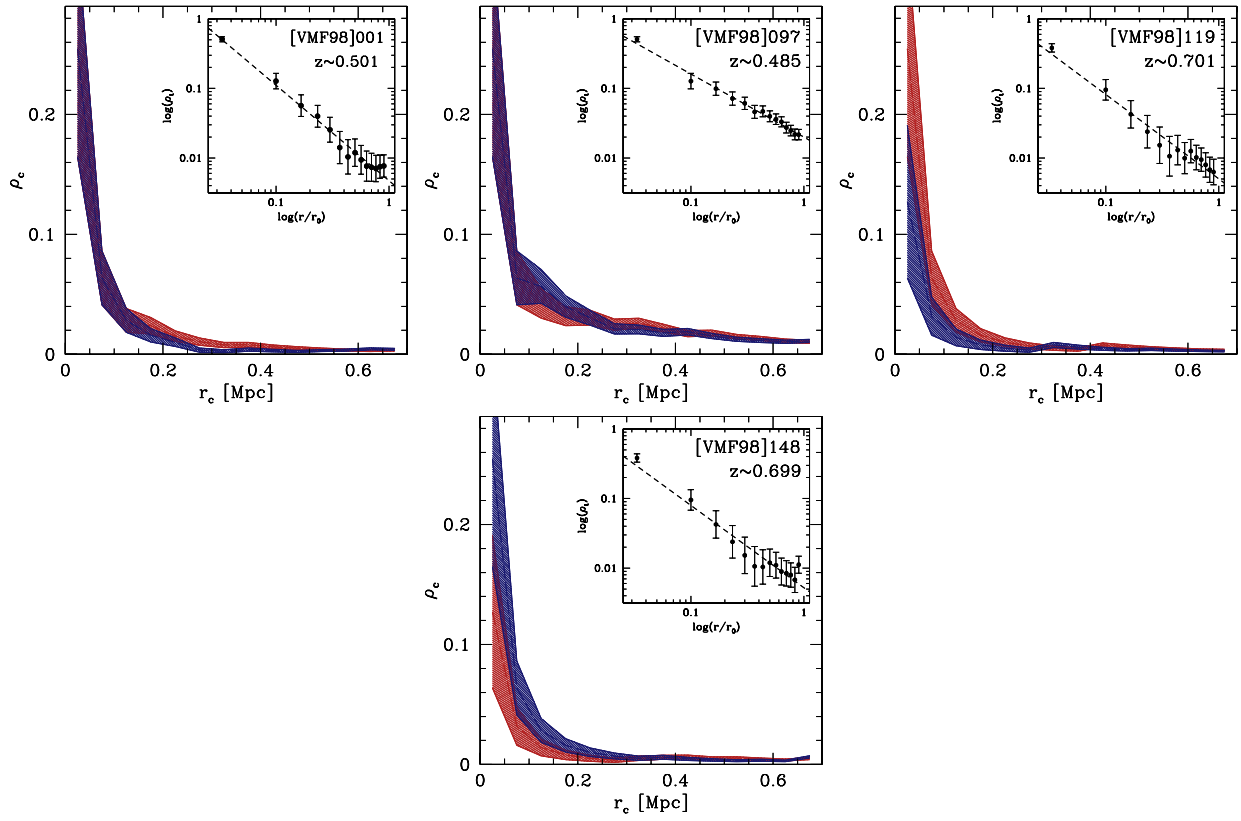

Figure 10. Galaxy number density profiles for the high-redshift galaxy clusters for the RCS and Blue samples. Panels and colours are as in previous figures.

we obtained the galaxy number counts and the CMRs of the clusters, including the RCS, galaxy colour distributions and the relative fraction of the blue galaxies. The galaxy radial density profiles and galaxy projected distributions were also obtained for our cluster sample.

At lower redshifts ($z < 0.4$), the main results presented in this paper can be summarized as follows.

(i) The presence of a well-defined RCS was found with an extension of at least 4 mag, characteristic of virialized systems with a dominant elliptical galaxy. We also encountered some galaxies with extreme colours around $(g - r)' \sim 0.8$ in [VMF98]124 and $(r - i)' \sim 0.37$ in [VMF98]093, which possibly indicate strong star formation related to cluster dynamics.

(ii) The clusters are dominated by a red population, with a peak at $(g - r)' \sim 1.33$ for [VMF98]124 and $(r - i)' \sim 0.64$ and 0.76 for [VMF]022 and [VMF98]093, respectively.

(iii) The galaxy density profiles show a central concentration for the RCS sample, with an absence of blue galaxies in the central region. Nearly 70 per cent of the red galaxies are located at the cluster core ($r_c < 200$ kpc).

At higher redshifts ($0.4 < z < 0.7$), the galaxy clusters studied revealed the following.

(i) A less important RCS with a smaller extension, but with a clear presence of the blue population.

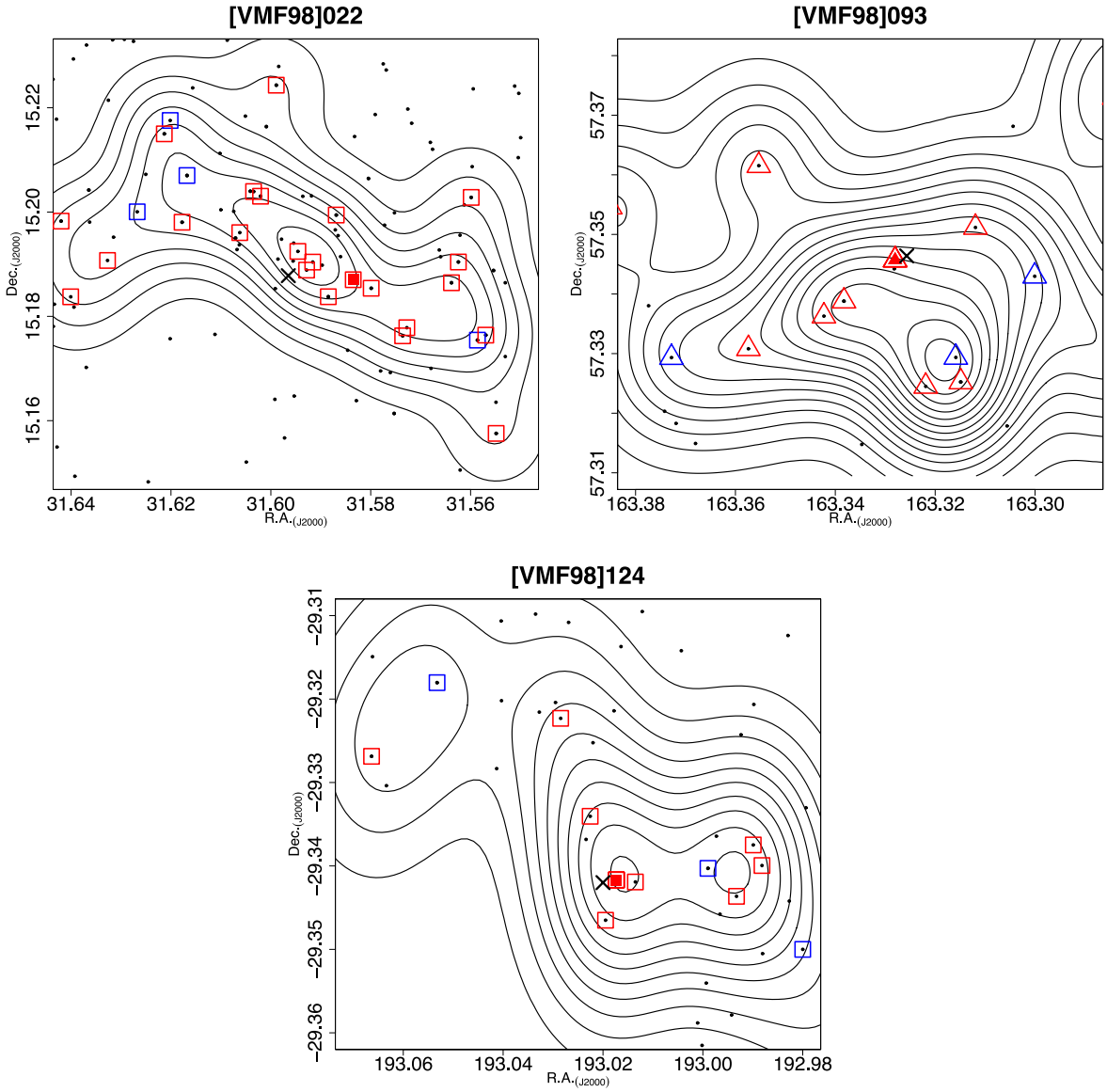

Figure 11. Galaxy density maps for the low-redshift galaxy clusters. Crosses indicate the position of the X-ray emission peak and filled symbols (both triangles and squares) show the BCG locus. Superposed to the contours are the RCS and Blue samples, with the foreground and background galaxies being represented by black dots.

(ii) A broader galaxy colour distribution with two peaks: the RCS and the blue population. A Gaussian function provided a good fit for both populations.

(iii) The total galaxy radial density profiles were well fitted by a single power law.

For the three galaxy clusters with spectroscopic measurements, no significant detection of substructures through the DST analysis was found.

The fractions of elliptical, lenticular and blue galaxies were calculated as a function of cluster redshift ($0.17 < z < 0.70$), confirming an increasing fraction of blue galaxies from 0.1 to 0.5 with redshift, a fact related to the Butcher–Oemler effect. As redshift increases, the fraction of lenticulars decreases from about 0.4 to 0.1, whereas the fraction of early types remains almost constant at about 0.35. In addition, the concentration index of cluster galaxies showed no strong dependence on redshift, except for [VMF98]124.

The seven galaxy clusters studied in this paper is only a fraction of a larger sample that will be addressed in forthcoming papers. In this sense, the trends reported for this small cluster sample are not sufficiently robust, so in future work we will attempt to consolidate these findings.

ACKNOWLEDGEMENTS

JLNC acknowledges the financial support from Consejo Nacional de Investigaciones Científicas y Técnicas de la República Argentina (CONICET). This work was partially supported by Consejo de Investigaciones Científicas y Técnicas (CONICET), Secretaría de Ciencia y Técnica (Secyt) of Universidad Nacional de Córdoba and Ministerio de Ciencia y Tecnología (MINCyT, Córdoba). We thank Dr Paul Hobson, native speaker, for revision of the manuscript.

SDSS-III is managed by the Astrophysical Research Consortium for the Participating Institutions of the SDSS-III Collaboration including the University of Arizona, the Brazilian

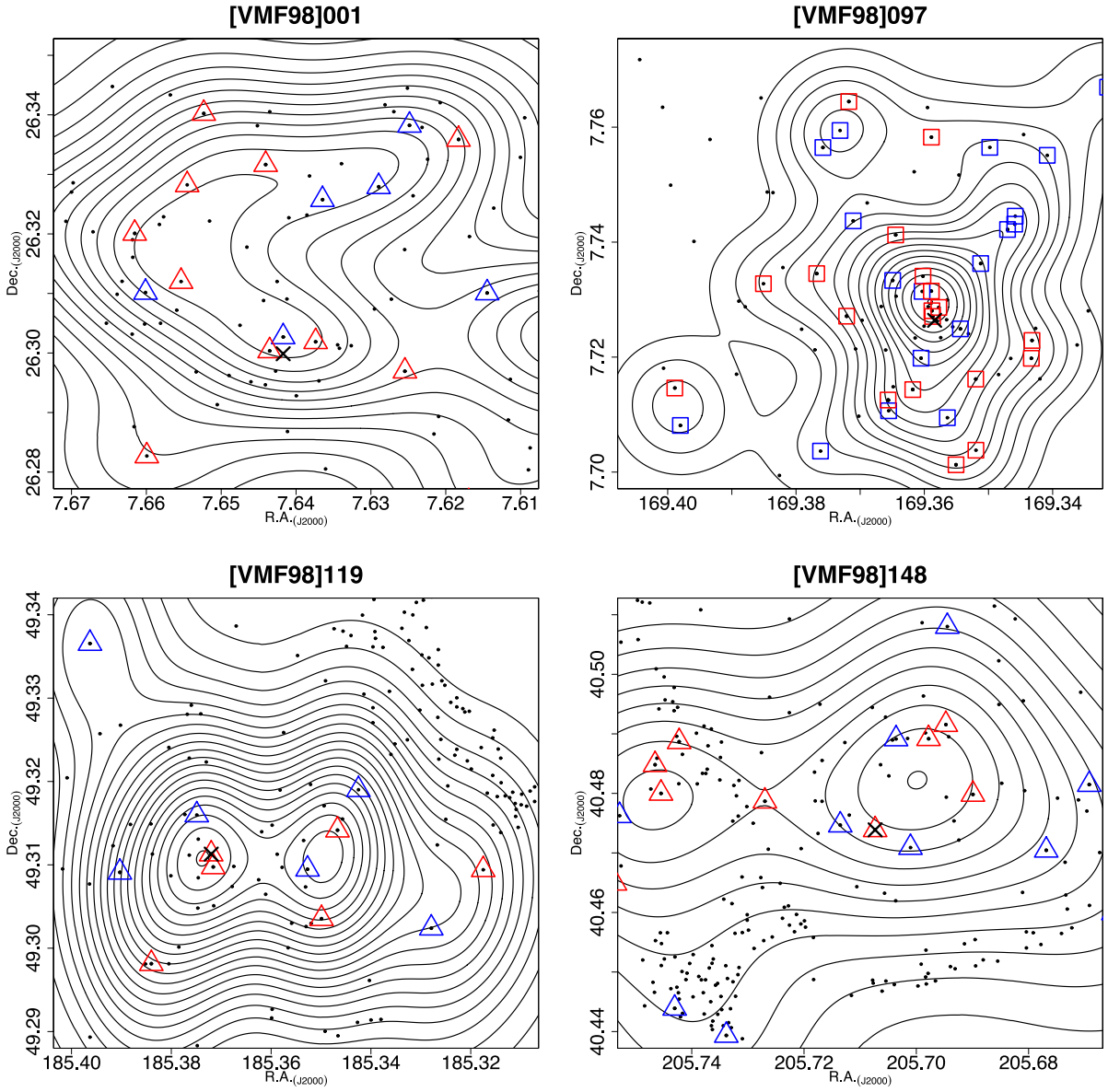

Figure 12. Galaxy density maps for the high-redshift galaxy clusters. Symbols are similar to previous figures.

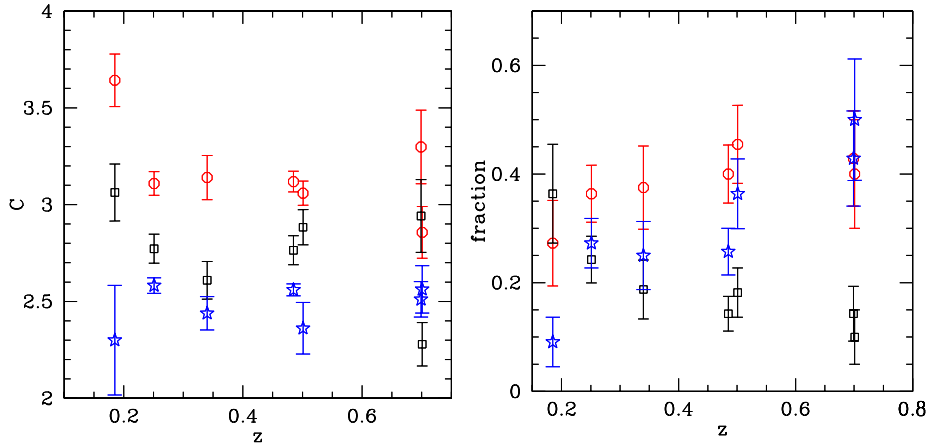

Figure 13. Morphological properties versus z for the studied galaxy clusters. Left-hand panel: mean concentration index for early (squares), lenticular (circles) and spiral (triangles) galaxies. Right-hand panel: morphological type fraction. Error bars are based on Poisson statistics.

Participation Group, Brookhaven National Laboratory, University of Cambridge, University of Florida, the French Participation Group, the German Participation Group, the Instituto de Astrofísica de Canarias, the Michigan State/Notre Dame/JINA Participation Group, Johns Hopkins University, Lawrence Berkeley National Laboratory, Max Planck Institute for Astrophysics, New Mexico State University, New York University, Ohio State University, Pennsylvania State University, University of Portsmouth, Princeton University, the Spanish Participation Group, University of Tokyo, University of Utah, Vanderbilt University, University of Virginia, University of Washington and Yale University.

REFERENCES

Aihara H. et al., 2011, ApJS, 193, 29
Balogh M., Bower R. G., Smail I., Ziegler B. L., Davies R. L., Gaztelu A., Fritz A., 2002, MNRAS, 337, 256
Balogh M. L. et al., 2009, MNRAS, 398, 754
Balogh M. L. et al., 2011, MNRAS, 412, 2303
Barrena R., Girardi M., Boschin W., de Grandi S., Eckert D., Rossetti M., 2011, A&A, 529, A128
Barrena R., Girardi M., Boschin W., Mardirossian F., 2012, A&A, 540, A90
Bernardi M., Sheth R. K., Nichol R. C., Schneider D. P., Brinkmann J., 2005, AJ, 129, 61
Bertin E., Arnouts S., 1996, A&AS, 117, 393
Boschin W., Girardi M., Spolaor M., Barrena R., 2006, A&A, 449, 461
Bruzual A. G., 1983, ApJ, 273, 105
Bruzual A. G., Kron R. G., 1980, ApJ, 241, 25
Butcher H., Oemler A., Jr, 1978, ApJ, 219, 18
Calvi R., Poggianti B. M., Vulcani B., 2011, MNRAS, 416, 727
Carrasco E. R., Mendes de Oliveira C., Infante L., 2006, AJ, 132, 1796
Carrasco E. R., Cypriano E. S., Neto G. B. L., Cuevas H., Sodré L., Jr, de Oliveira C. M., Ramirez A., 2007, ApJ, 664, 777
Cohn J. D., 2012, MNRAS, 419, 1017
Connelly J. L. et al., 2012, ApJ, 756, 139
Conselice C. J., 2003, ApJS, 147, 1
Conselice C. J., Bershady M. A., Jangren A., 2000, ApJ, 529, 886
Conselice C. J., Rajgor S., Myers R., 2008, MNRAS, 386, 909
De Lucia G. et al., 2004, ApJ, 610, L77
De Lucia G., Springel V., White S. D. M., Croton D., Kauffmann G., 2006, MNRAS, 366, 499
De Lucia G. et al., 2007, MNRAS, 374, 809
Demarco R. et al., 2010, ApJ, 711, 1185
Dressler A., Shectman S. A., 1987, AJ, 94, 899
Dressler A., Shectman S. A., 1988, AJ, 95, 985
Dressler A. et al., 1997, ApJ, 490, 577
Dressler A., Oemler A., Gladders M. G., Bai L., Rigby J. R., Poggianti B. M., 2009, ApJ, 699, L130
Einasto M. et al., 2012, A&A, 540, A123
Ellis R. S., Smail I., Dressler A., Couch W. J., Oemler A., Jr, Butcher H., Sharples R. M., 1997, ApJ, 483, 582
Fairley B. W., Jones L. R., Wake D. A., Collins C. A., Burke D. J., Nichol R. C., Romer A. K., 2002, MNRAS, 330, 755
Fasano G., Poggianti B. M., Couch W. J., Bettoni D., Kjærgaard P., Moles M., 2000, ApJ, 542, 673
Frei Z., Gunn J. E., 1994, AJ, 108, 1476
Fukugita M., Shimasaku K., Ichikawa T., 1995, PASP, 107, 945
Gallazzi A., Charlot S., Brinchmann J., White S. D. M., 2006, MNRAS, 370, 1106
Gilbank D. G., Yee H. K. C., Ellingson E., Gladders M. D., Loh Y.-S., Barrientos L. F., Barkhouse W. A., 2008, ApJ, 673, 742
Girardi M., Barrena R., Boschin W., Ellingson E., 2008, A&A, 491, 379
Girardi M., Bardelli S., Barrena R., Boschin W., Gastaldello F., Nonino M., 2011, A&A, 536, A89
Gladders M. D., Yee H. K. C., 2005, ApJS, 157, 1
Gladders M. D., López-Cruz O., Yee H. K. C., Kodama T., 1998, ApJ, 501, 571
Hansen S. M., McKay T. A., Wechsler R. H., Annis J., Sheldon E. S., Kimball A., 2005, ApJ, 633, 122
Hao J. et al., 2010, ApJS, 191, 254
Hashimoto Y., Oemler A., Jr, 1999, ApJ, 510, 609
Hook I. M., Jørgensen I., Allington-Smith J. R., Davies R. L., Metcalfe N., Murowinski R. G., Crampton D., 2004, PASP, 116, 425
Hou A., Parker L. C., Harris W. E., Wilman D. J., 2009, ApJ, 702, 1199
Jeltema T. E., Mulchaey J. S., Lubin L. M., Rosati P., Böhringer H., 2006, ApJ, 649, 649
Kauffmann G., Charlot S., 1998, MNRAS, 294, 705
King C. R., Ellis R. S., 1985, ApJ, 288, 456
Kinney A. L., Calzetti D., Bohlin R. C., McQuade K., Storchi-Bergmann T., Schmitt H. R., 1996, ApJ, 467, 38
Knebe A., Müller V., 2000, A&A, 354, 761
Kodama T., Arimoto N., 1997, A&A, 320, 41
Kodama T., Bower R. G., 2001, MNRAS, 321, 18
Landolt A. U., 1992, AJ, 104, 340
Lerchster M. et al., 2011, MNRAS, 411, 2667
López-Cruz O., Barkhouse W. A., Yee H. K. C., 2004, ApJ, 614, 679
McIntosh D. H., Rix H.-W., Caldwell N., 2004, ApJ, 610, 161
Mei S. et al., 2006a, ApJ, 639, 81
Mei S. et al., 2006b, ApJ, 644, 759
Mei S. et al., 2009, ApJ, 690, 42
Metcalfe N., Shanks T., Campos A., McCracken H. J., Fong R., 2001, MNRAS, 323, 795
Mullis C. R. et al., 2003, ApJ, 594, 154
Mullis C. R., Rosati P., Lamer G., Böhringer H., Schwope A., Schuecker P., Fassbender R., 2005, ApJ, 623, L85
Nagashima M., Yoshii Y., Totani T., Gouda N., 2002, ApJ, 578, 675
Nilo Castellon J. L., Alonso M. V., 2013, available at: http://www.dfuls.cl/XGClusters/
Nilo Castellón J. L. et al., 2013, MNRAS, submitted (Paper I)
O'Mill A. L., Duplancic F., García Lambas D., Valotto C., Sodré L., 2012, MNRAS, 421, 1897
Poggianti B. M. et al., 2009, ApJ, 697, L137
Press W. H., Teukolsky S. A., Vetterling W. T., Flannery B. P., 1992, Numerical Recipes in FORTRAN. The Art of Scientific Computing, 2nd edn. Cambridge Univ. Press, Cambridge
Sarazin C. L., 1986, Rev. Mod. Phys., 58, 1
Schlegel D. J., Finkbeiner D. P., Davis M., 1998, ApJ, 500, 525
Secker J., Harris W. E., Plummer J. D., 1997, PASP, 109, 1377
Stanford S. A., Eisenhardt P. R., Dickinson M., 1998, ApJ, 492, 461
Stott J. P., Pimbblet K. A., Edge A. C., Smith G. P., Wardlow J. L., 2009, MNRAS, 394, 2098
Strateva I. et al., 2001, AJ, 122, 1861
Terlevich A. I., Caldwell N., Bower R. G., 2001, MNRAS, 326, 1547
Tonnesen S., Bryan G. L., 2009, ApJ, 694, 789
Tran K.-V. H., Franx M., Illingworth G. D., van Dokkum P., Kelson D. D., Blakeslee J. P., Postman M., 2007, ApJ, 661, 750
van den Bergh S., 2001, AJ, 122, 621
van Dokkum P. G., Franx M., Kelson D. D., Illingworth G. D., Fisher D., Fabricant D., 1998, ApJ, 500, 714
Vikhlinin A., McNamara B. R., Forman W., Jones C., Quintana H., Hornstrup A., 1998, ApJ, 502, 558
Visvanathan N., Sandage A., 1977, ApJ, 216, 214
Vulcani B., Poggianti B. M., Finn R. A., Rudnick G., Desai V., Bamford S., 2010, ApJ, 710, L1
Wake D. A., Collins C. A., Nichol R. C., Jones L. R., Burke D. J., 2005, ApJ, 627, 186
White M., Cohn J. D., Smit R., 2010, MNRAS, 408, 1818
Yamauchi C. et al., 2005, AJ, 130, 1545
Yee H. K. C., Gladders M. D., López-Cruz O., 1999, ASP Conf. Ser. Vol. 191, Photometric Redshifts and the Detection of High Redshift Galaxies. Astron. Soc. Pac., San Francisco, p. 166

This paper has been typeset from a TEX/LATEX file prepared by the author.